Phase transformations and precipitation in amorphous $Ti_{50}Ni_{25}Cu_{25}$ ribbons

C. Satto [a], A. Ledda [a], P. Potapov [a], J.F. Janssens [b], D. Schryvers [a,*]

[a]*Electron Microscopy for Materials Research (EMAT), University of Antwerp, RUCA, Groenenborgerlaan 171, B-2020 Antwerp, Belgium*
[b]*Chemistry Department, University of Antwerp, RUCA, Groenenborgerlaan 171, B-2020 Antwerp, Belgium*

Abstract

Phase transformations and precipitation mechanisms in $Ti_{50}Ni_{25}Cu_{25}$ material, starting from an amorphous planar-cast ribbon, were studied by in-situ transmission electron microscopy (TEM). On heating, the cubic B2 austenite crystallisation occurs around 470°C after which the orthorhombic B19 martensite is formed on cooling. Annealings up to 700°C yield the identification of Cu_3Ti_2 and Ti_2Ni precipitates. These precipitations drastically alter the matrix composition, resulting in the formation upon cooling of the monoclinic B19′ martensite with different types of long-period stacking sequences. Also the B19′ martensite is still recognised in the latter samples. © 2001 Elsevier Science Ltd. All rights reserved.

Keywords: A. Ternary alloy systems; B. Martensitic transformations; B. Phase transformations

1. Introduction

TiNi alloys are well known for their excellent shape-memory properties, as well as for their superelastic behaviour. Alloying with ternary elements can severely affect the transformation, for example the substitution of Cu for Ni changes the martensite start temperature M_s as well as the martensite structure [1]. The phase diagram of $Ti_{50}Ni_{50-x}Cu_x$ [2] is reproduced in Fig. 1. For low Cu concentration the monoclinic martensite B19′ is formed on cooling, similar to the transformation in the equiatomic binary compound [3]. For a Cu content around 10 at.%, the orthorhombic B19 martensite appears as an intermediate phase towards B19′ formation (B2→B19→B19′), the width of the composition region increasing with decreasing temperature [4–6]. Higher Cu levels inhibit the second step of this transformation and only B19 is retained [7,8].

The emphasis of the present work is on the in-situ observation by transmission electron microscopy (TEM) of the different transformation processes that take place when a ternary amorphous planar-cast ribbon with a composition of $Ti_{50}Ni_{25}Cu_{25}$ (at.%) is heated. Contrary to most other investigations, our anneals were performed up to 700°C and the effects compared with those in the more classic treatment up to 500°C.

2. Experimental

The starting material is an amorphous ribbon prepared from a melt of $Ti_{50}Ni_{25}Cu_{25}$ by the planar casting technique applied under argon atmosphere, which yields a cooling rate of $\sim 5 \times 10^5$ K/s. The resulting ribbons have a thickness of approximately 40 μm. TEM samples were obtained by punching 3 mm diameter samples from the ribbons and mechanically polishing them to a thickness of 20 μm. These samples were further electro-polished, at room temperature, using an acetic acid solution with 8% of perchloric acid [9].

Conventional TEM images and selected area electron diffraction patterns were obtained in a Philips CM20 microscope. This latter is equipped with an energy dispersive X-ray spectrometry (EDX) device and a double-tilt heating holder. Differential scanning calorimetry (DSC) measurements were performed using a TA instrument 2920, operating under a nitrogen flux of 50

---

* Corresponding author. Tel.: +32-3-218-0247; fax: +32-3-218-0257.

E-mail address: schryver@ruca.ua.ac.be (D. Schryvers).
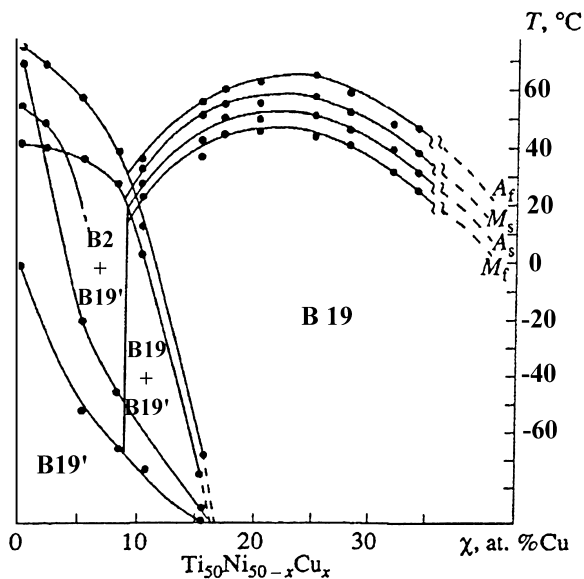
Fig. 1. Phase diagram of $Ti_{50}Ni_{50-x}Cu_x$ showing the effect of Cu addition on the martensite structure and transformation temperatures [2].

ml/min, with an alumina crucible holding the sample and using an empty alumina crucible as a reference.

3. Results

3.1. Heating treatment up to 500°C

Fig. 2a shows the early state of the B2 austenite crystallisation of spherical particles. These finally grow into well crystallised micron-sized grains of B2 at 500°C, as

seen in Fig. 2b. From the DSC analysis, crystallisation was determined to start at 450°C and was completely finished at 490°C. Cooling the crystallised material inside the microscope at a rate of 10°C/min yields the martensitic transformation with the formation of the orthorhombic B19 phase, as revealed by SAED patterns corresponding to the [30-1] and [10-1] orientations and shown in Fig. 3a and b, respectively. All martensite grains show a twinned morphology as clearly seen from Fig. 3c. The B19 orthorhombic martensite crystallises in the *Pmmb* space group, with cell parameters $a = 0.29177(6)$ nm, $b = 0.42900(8)$ nm and $c = 0.45039(8)$ nm, determined by X-ray diffraction refinement in a separate study focussing on this annealing treatment [10]. These results confirm earlier studies on similar materials [11,12]. No fine-scale long-period twin sequences resulting in super-reflections in the SAED patterns of the martensite were found in these samples.

Here it is worth mentioning that the thinning, necessary for obtaining transparent TEM samples, strongly affects the material's response. Indeed, in the thinnest edges of the TEM sample, only very small (i.e. with dimensions between 10 and 100 nm) austenite grains are formed. These small grains usually do not transform to the martensite structure upon in-situ cooling in the microscope. As a result, structural studies of the martensites thus have to be performed in samples heated before the electropolishing/thinning procedure.

3.2. Heating treatment up to 700°C

Continuing the heating treatment after the crystallisation to temperatures higher than 500°C induces
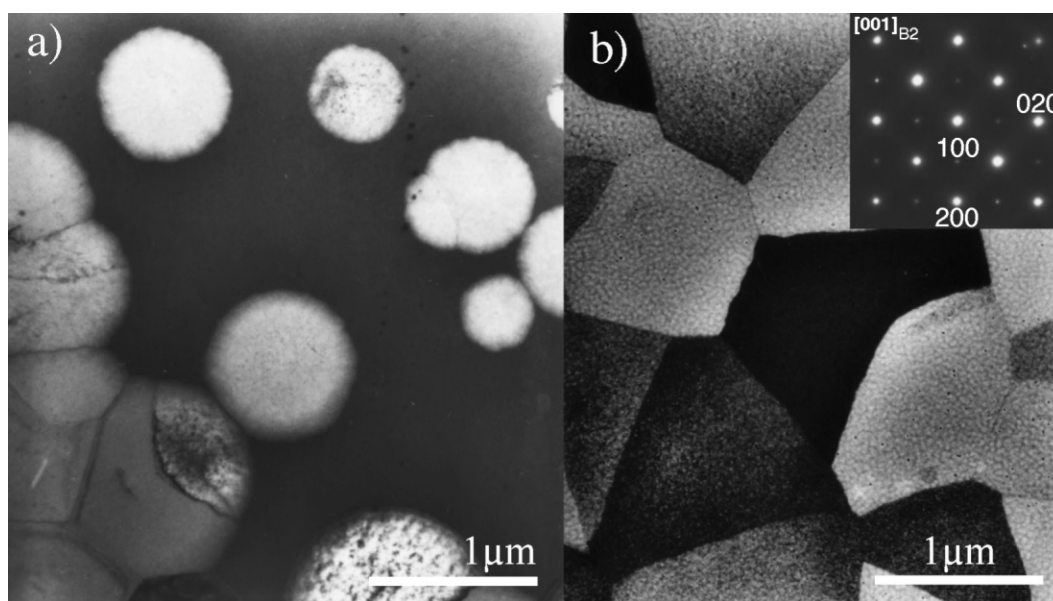
Fig. 2. TEM images of (a) start of the B2 crystallisation at 480°C and (b) micron-sized B2 grains at 500°C. The inset SAED pattern clearly reveals the B2 type structure.
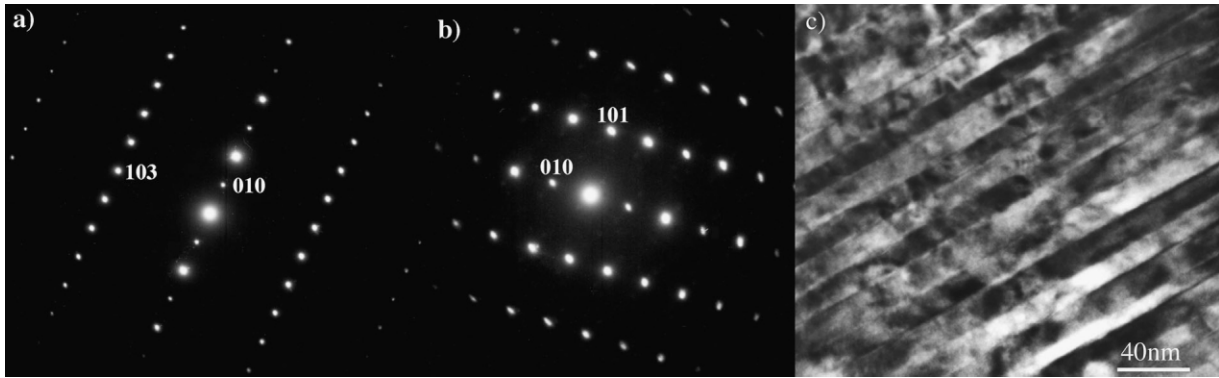
Fig. 3. SAED patterns of B19 in (a) [30-1], (b) [10-1] zone orientation and (c) twinned morphology of the martensite B19 plates.

precipitation at around 600°C, as shown in Fig. 4a. Particles of a maximum size of 100 nm at 700°C are seen to form inside the grains as well as at the grain boundaries, strongly disturbing the geometrical image of the grains. As evidenced by the contrast of the particle labelled A in Fig. 4b, the larger particles are sometimes multigrained. Their chemical composition, determined by EDX analysis, corresponds, on average, to 50 at.% Cu, 40 at.% Ti and 10 at.% Ni. Assuming a single sublattice with a random occupation for Cu and Ni, these particles could present the tetragonal Cu_3Ti_2 structure with space group $P4/nmm$ and cell parameters close to $a = 0.313$ nm, $c = 1.395$ nm, values known for the stoichiometric compound [13]. This hypothesis was confirmed by the observation of diffraction patterns as in the inset of Fig. 4b, which can be indexed as the [56-1] zone of Cu_3Ti_2. The present pattern furthermore allows

the characterisation of twinning along the (105) plane, responsible for the contrast in particle A of Fig. 4b.

Occasionally, evidence from a cubic superstructure with cell parameter $a = 1.127$ nm was found, as shown in the SAED pattern of Fig. 5. Although the relevant reflections at short reciprocal distances are weak and no full diffraction study could be performed owing to the elevated temperature and small sizes of the precipitates involved, these observations do indicate the presence of very small particles with the Ti_2Ni structure [14,15].

On cooling, the martensitic transformation occurs around 50°C, the temperatures of transformation being determined accurately by DSC measurements of unthinned material. Moreover, these measurements indicate that the martensitic transformation occurs in two steps, as clearly evidenced by the two peaks in the DSC curve of Fig. 6. From the TEM experiments it was found that
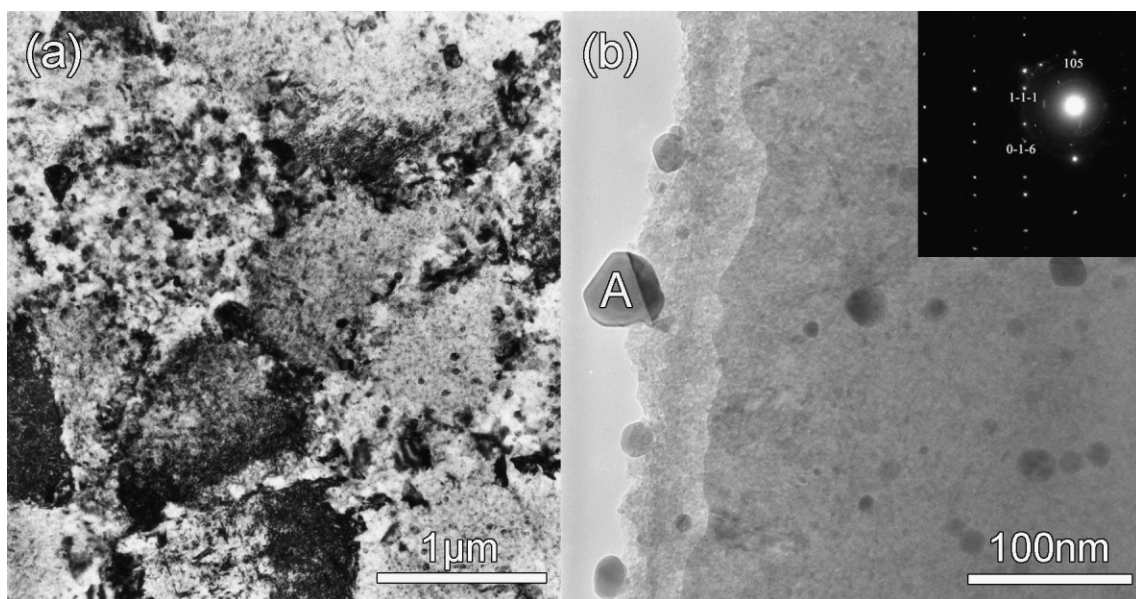
Fig. 4. (a) Beginning of the precipitation at 600°C and (b) multigrained precipitates at 700°C with the inset revealing twinning in the [56-1] zone of a Cu_3Ti_2 particle.
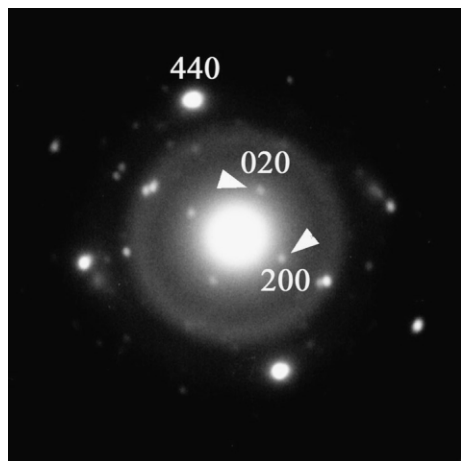
Fig. 5. SAED pattern revealing evidence for the existence of Ti_2Ni particles.

not only the orthorhombic B19 martensite appears, but also the B19′ type (space group $P2_1/m$, cell parameters $a = 0.2898$ nm, $b = 0.4108$ nm, $c = 0.4646$ nm and $\beta = 97.78°$ [16]), obtained by a monoclinic distortion of B19. A typical [100] diffraction pattern of B19′ is shown in Fig. 7. It reveals an (011) type I twinning (underlined indexations) superposed by a six-fold stacking sequence of (011) twin planes, already well-known in the B19 [17] as well as B19′ case [18].

Local EDX measurements of the martensite plates yield an average composition of $Ti_{50}Ni_{40}Cu_{10}$. Due to the strong mixing of B19 and B19′ regions, no separate compositions could be obtained for the two martensite structures.

As most structures appear with relatively small-sized morphologies, the final room temperature microstructure is a complex combination of different crystallographic structures and variants. Each austenite grain is divided into several twinned martensite plates, with numerous untransformed precipitates still distributed inside and between them, resulting in bright field images as in Fig. 8. A typical example of an SAED pattern from such a region is shown in Fig. 9a. The point-like reflections, indicated by vertical arrows, can be explained by the Cu_3Ti_2 structure in the [56-1] orientation, twinned along (105). The remaining reflections appear to belong to a superstructure. They show slight streaking along the reciprocal direction of the superstructure and appear at commensurate or incommensurate locations, depending on the actual pattern.

A first possible explanation is by attributing these reflections to twinning along (001) of the B19′ monoclinic martensite, here observed along its [110] orientation. This type of twinning is indeed well known for the monoclinic B19′ structure [18,19] and is evidenced by the doublet of strong (111) type reflections, as shown in Fig. 9b. The streaked reflections at (in)commensurate positions around 1/3 of the basic reflections would then correspond to an imperfect superstructure or modulation of the monoclinic twinning. This interpretation is further sustained by the occasional observation of a [110] orientation of the B19 structure superposed on the pattern of Fig. 9a, yielding unsplit $(111)_{B19}$ type reflections in between the twinned monoclinic ones. However, this explanation is not fully convincing because of small discrepancies in the values of the angles when compared with the regular monoclinic unit cell and the absence of the (001) reflection. Still, a superstructure could imply a slightly different monoclinic angle and a longitudinal component of the modulation could yield a severe diminishing of the intensity of the 001 ordering reflection due to dynamical scattering.

The second possibility, simulated in Fig. 9c, consists of twinning along (111) of the [7-3-4] zone axis of a Ti_2Ni particle. Although this better explains the location and angles for the reflections in the second row, it is
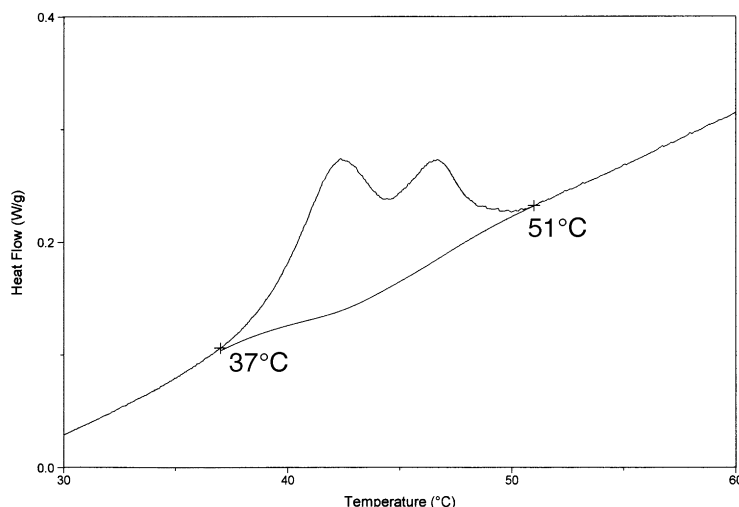
Fig. 6. DSC measurement indicating a two-step martensitic transformation upon cooling.
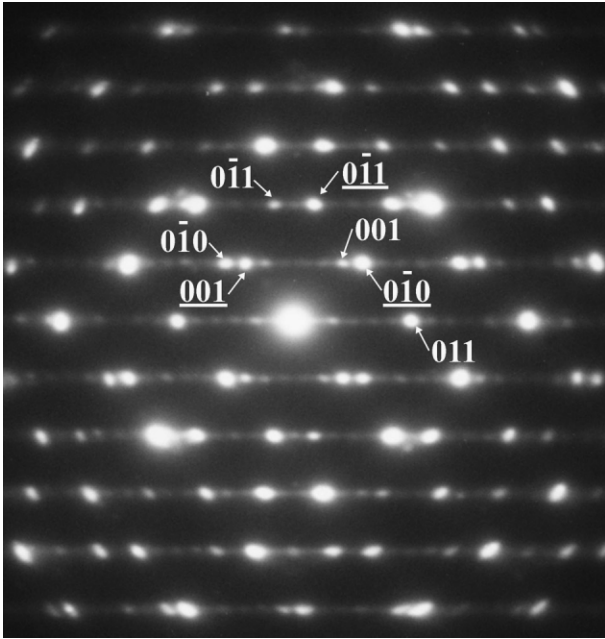
Fig. 7. [100] Zone axis of the B19′ martensite, showing long-period twinning along (011).
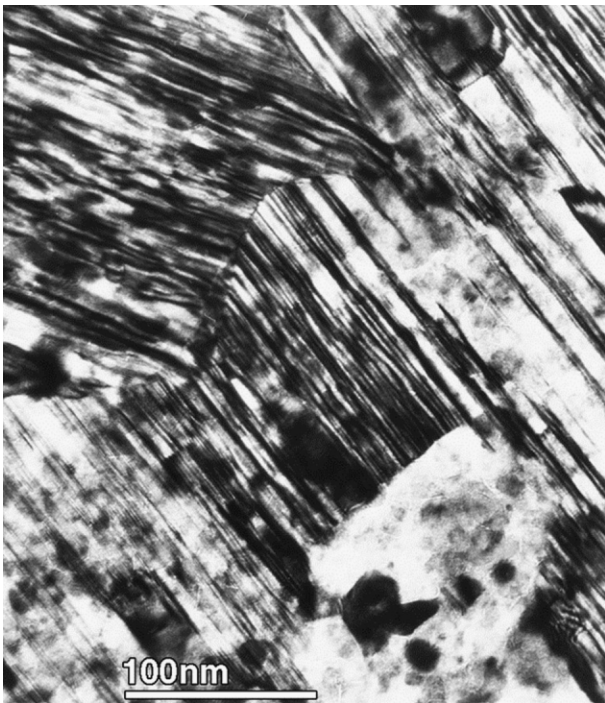
Fig. 8. Morphology of thin martensite plates together with retained precipitates.

in disagreement with the reflection conditions induced by the Fd-3m space group of the binary structure (hkl, $h + k = 2n$, $h + l = 2n$, $k + l = 2n$) which do not allow for the reflections in the first row. A chemical substitution, for instance some Cu in Ni sites, leading to

crystallisation with a lower symmetry space group, could, however, result in the appearance of these reflections.

Unfortunately, because of the very small size of the Ti_2Ni particles, no suitable EDX experiments could be performed. Still, this suggestion does not explain the occasional incommensurability of the streaked reflections at the 1/3 positions. The streaking itself could result from a plate-like shape of the precipitates.

Because of the high sensitivity of the martensite phase stability to observation under high energy electrons, no high resolution microscopy could be performed to elucidate this remaining problem.

4. Discussion

As precipitation takes place at temperatures above 500°C, the chemical composition of the austenite is changed and as a consequence also the chemical composition of the martensite formed by a purely displacive mechanism upon cooling. The observed precipitates are based on Cu_3Ti_2 and Ti_2Ni structures, but, certainly for the former, are appearing here as a ternary compound. These observations are in accordance with the starting chemical composition, $Ti_{50}Ni_{25}Cu_{25}$, which can also be written as $Ti_6Ni_3Cu_3$. In order to equilibrate the chemical equation (and first disregarding the ternary nature of the precipitates), two parts of the matrix with TiNi composition have to be introduced, as shown below. Then, when replacing Cu_3Ti_2 by the more accurate $Cu_{50}Ni_{10}Ti_{40}$ composition as determined by EDX, some Ni in the matrix has to be substituted by Cu. Thus, the martensite has a composition closer to $Ti_{50}Ni_{40}Cu_{10}$, probably by Cu substitution on Ni crystallographic sites, and the chemical balance between the precipitates and the matrix is retained. As the result of the decrease of Cu concentration in the matrix, the B19′ martensite structure is observed, in accordance with the phase diagram of Fig. 1.

$$Ti_{50}Ni_{25}Cu_{25}$$
$$\updownarrow$$
$$Ti_6Ni_3Cu_3 \longrightarrow Cu_3Ti_2 + Ti_2Ni + 2\ TiNi$$
$$\updownarrow \qquad\qquad\qquad \updownarrow$$
$$Cu_{50}Ni_{10}Ti_{40} \qquad Ti_{50}Ni_{40}Cu_{10}$$
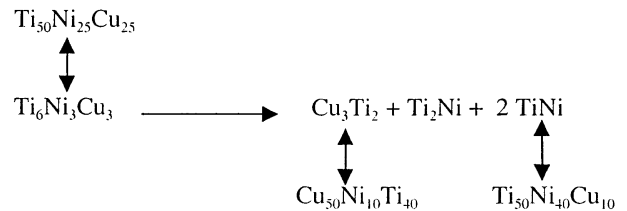
The fact that both B19 and B19′ martensite structures are observed at room temperature could imply that the entire matrix is relatively homogeneous with a Cu content close to 10 at.%. This then means that at least part of the two peaks in the DSC curve of Fig. 6 is due to a subsequent B2- > B19- > B19′ transformation. However, if the matrix is severely inhomogeneous as the result of the different precipitation processes, then the entire material could cover the different sequences as seen from the phase diagram in Fig. 1. In this case the two peaks in Fig. 6
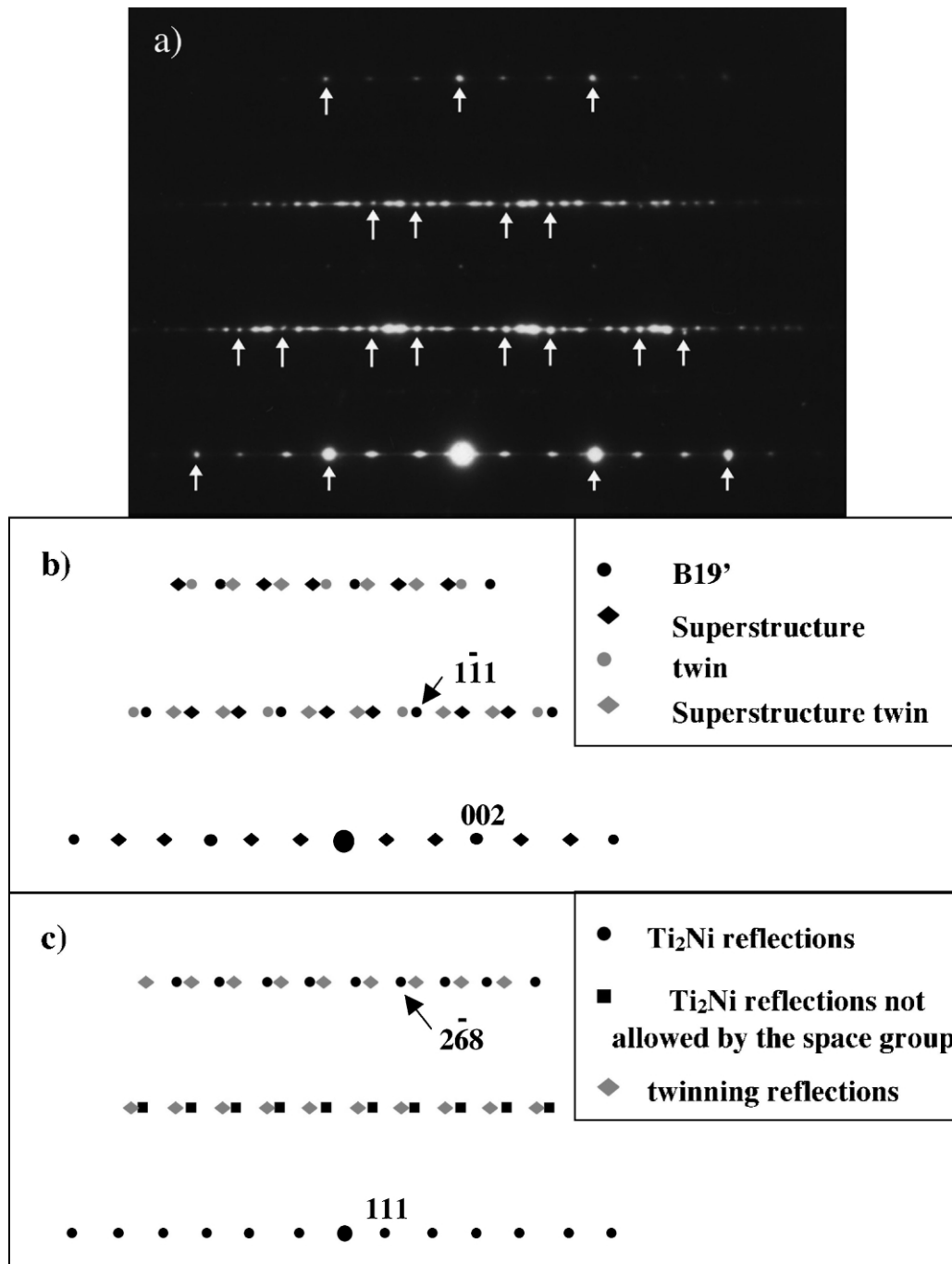
Fig. 9. (a) SAED pattern with indication of reflections belonging to the Cu_3Ti_2 structure in [56-1] orientation, twinned along (105) (vertical arrows); (b) schematic of (a) using [110] B19′ orientation twinned along (001) with a three-fold superstructure; and (c) schematic of (a) using [7-3-4] Ti_2Ni orientation, twinned along (111).

could well indicate two separate B2->B19 and B2->B19′ paths.

Regardless of the final conclusion on the complete elucidation of the transformation paths and the complex SAED patterns as in Fig. 9, the well aligned superposed reciprocal directions indicate that there is a strong crystallographic relation between the austenite and the precipitates and thus also with the martensite.

Indeed, as the [001] directions of the B19 and B19′ martensites originate from a <110> direction in the austenite [20], the [105] and [111] directions of the Cu_3Ti_2 and Ti_2Ni precipitates, respectively, also align with a <110> direction of the austenite. The formation of coherent precipitates is of considerable interest to potential applications as it is known to introduce the two-way shape memory behaviour of these materials [21].

5. Conclusion

The martensitic transformation in planar-cast $Ti_{50}Ni_{25}Cu_{25}$ ribbons annealed at different temperatures has been investigated by in-situ TEM. A heat treatment at 700°C leads to Cu_3Ti_2 and Ti_2Ni type precipitation, which changes the chemical composition of the austenite, in such a way that not only the orthorhombic martensite B19 is formed but also the monoclinic B19′, in accordance with the phase diagram. At least one and possible two distinct long-period microtwinned stacking sequences have been recognised in the B19′ martensite.

Acknowledgements

References

[1] Mercier O, Melton KN. Metall Trans 1979;10A:387.
[2] Van Loo FJJ, Bastin GF, Leenen AJH. J Less-Common Metals 1978;57:111.
[3] Michal GM, Sinclair R. Acta Cryst B 1981;37:1803.
[4] Nam TH, Saburi T, Shimizu K. Mater Trans JIM 1990;31:959.
[5] Nam TH, Saburi T, Kawamura Y, Shimizu K. Mater Trans JIM 1990;31:262.
[6] Lo YC, Wu SK, Horng HE. Acta Metall Mater 1993;41:747.
[7] Nam TH, Saburi T, Nakata Y, Shimizu K. Mater Trans JIM 1990;31:504.
[8] Bricknell RH, Melton KN, Mercier O. Metall Trans 1979;10A:693.
[9] Zel'dovich V, Sobyanina G, Novoselova TV. Journal de Physique IV 1997;7:299.
[10] Potapov PL, Shelyakov AV, Schryvers D. Scripta Mater, in press.
[11] Rösner H, Shelyakov AV, Glezer AM, Feit K, Schlobmacher P. Materials Science and Engineering 1999;A273-275:733.
[12] Nishida M, Ohgi H, Itai I, Chiba A, Yamauchi K. Trans Mater Res Soc Jpn 1994;18R:1073.
[13] Schubert K. Z fr Metallkunde 1965;56:197.
[14] Matsunaga T, Kajiwara S, Ogawa K, Kikuchi T, Miyazaki S. Materials Science Forum 2000;327-328:175.
[15] Kawamura Y, Gyobu A, Saburi T, Asai M. Materials Science Forum 2000;327-328:303.
[16] Pushin VG, Volkova SB, Matveeva NM, Yurchenko LI, Chistyakov AS. Physics of Metals and Metallography 1997;84:441.
[17] Xie ZL, Van Humbeek J, Liuand Y, Delaey L. Scripta Mater 1997;37:363.
[18] Nishida M, Li S. Materials Science Forum 2000;327-328:103.
[19] Liuwen C, Grummon DS. Phil Mag 1997;A76:191.
[20] Otsuka K, Ren X. Intermetallics 1999;7:511.
[21] Liu Y, McCormick PG. Acta Metall 1989;37:1321.